

Searching for Axion-Like Particles with the Blazar Observations of MAGIC and *Fermi*-LAT

Hai-Jun Li,^{1,2,3} Xiao-Jun Bi,^{2,3} and Peng-Fei Yin²

¹*Center for Advanced Quantum Studies, Department of Physics,
Beijing Normal University, Beijing 100875, China*

²*Key Laboratory of Particle Astrophysics, Institute of High Energy Physics,
Chinese Academy of Sciences, Beijing 100049, China*

³*School of Physics, University of Chinese Academy of Sciences, Beijing 100049, China*

(Dated: January 10, 2022)

We explore the axion-like particle (ALP)-photon oscillation effect in the γ -ray spectra of the blazars Markarian 421 (Mrk 421) and PG 1553+113, which are measured by the Major Atmospheric Gamma Imaging Cherenkov Telescopes (MAGIC) and *Fermi* Large Area Telescope (*Fermi*-LAT) with high precision. We investigate the constraints on the ALP parameter space using the Mrk 421 and PG 1553+113 observations of 15 and 5 phases, respectively. We find that the combined analysis with all the 15 phases improves the limits from the Mrk 421 observations. The combined limit set by the Mrk 421 observations has excluded the ALP parameter region with the ALP-photon coupling of $g_{a\gamma} \gtrsim 2 \times 10^{-11} \text{ GeV}^{-1}$ for the ALP mass of $\sim 8 \times 10^{-9} \text{ eV} \lesssim m_a \lesssim 2 \times 10^{-7} \text{ eV}$ at 95% C.L. We also find that the ALP hypothesis can slightly improve the fit to the PG 1553+113 results in some parameter regions, and do not set the limit in this case.

I. INTRODUCTION

The strong CP problem is a long standing puzzle in the Standard Model (SM) with the tiny value of $\bar{\theta} \lesssim 10^{-10}$. Introducing an additional spontaneously broken $U(1)$ symmetry, which is also broken by the anomaly at the quantum level, can elegantly solve the strong CP problem [1, 2]. This mechanism predicts a light pseudo Nambu-Goldstone boson, called quantum chromodynamics (QCD) axion [3, 4]. The axion is also a suitable candidate of cold dark matter. In the early universe, these particles can be nonthermally produced via the misalignment mechanism or the decays of topological defects [5–9].

The interactions between the axion and SM particles, such as the photons, leptons, and nucleons, can be described by the effective operators. In the QCD axion models, the axion mass and its couplings to the SM particles are related. From the experimental perspective, searching for the more general parameter space is well motivated. The corresponding particles have the similar effective interactions as the QCD axion, but do not have to solve the strong CP problem. Such particles are the so called axion-like particles (ALPs), which are also well motivated in some new physics models beyond the SM, such as the string models [10–12].

The ALPs have been searched in numerous laboratory and astrophysical experiments for a long time. If the ALP has the coupling to the photons, the ALP and free photon may convert to each other in the external magnetic field [13]. The astrophysical magnetic fields on the large scale would induce a detectable ALP-photon oscillation effect. For the astrophysical source at a large distance, this effect would modify the measured photon spectrum [14, 15]. In the literature, many studies have been performed to investigate this effect based on the observations

of different sources [14–51]. Since no ALP effect has been found, these analyses set limits on the ALP mass m_a and the ALP-photon coupling $g_{a\gamma}$ parameter space.

The ALP implication of the high energy γ -ray spectra of the blazars PKS 2155–304 and PG 1553+113, which are measured by H.E.S.S. and *Fermi* Large Area Telescope (*Fermi*-LAT) [52] during the common operation time, is investigated in Ref. [43]. The ALP-photon conversion in the turbulent inter-cluster magnetic field $\sim \mathcal{O}(1) \mu\text{G}$ is considered. The ALP-photon conversion in the blazar jet magnetic field (BJMF) of Markarian 421 (Mrk 421) is explored in Ref. [45]. The Astrophysical Radiation with Ground-based Observatory at Yang-BaJing (ARGO-YBJ) and *Fermi*-LAT results covering 10 phases of Mrk 421 [53] are combined together to set the constraint on the ALP parameter space. Compared with the constraint derived from the individual phase, the combined constraint is significantly improved.

In this work, we use the very high energy (VHE) γ -ray spectra of Mrk 421 and PG 1553+113 measured by the Major Atmospheric Gamma Imaging Cherenkov Telescopes (MAGIC) [54] to investigate the ALP-photon oscillation effect. Compared with Ref. [43], we study the ALP-photon conversion in the BJMF of PG 1553+113 in this analysis. Compared with the VHE measurements used in previous studies [43, 45], the MAGIC measurements cover more phases (15 phases for Mrk 421 and 5 phases for PG 1553+113) with high precision. Additionally, the γ -ray spectra of the blazars at lower energies ($\sim 0.1 - 100 \text{ GeV}$) can be well constrained by the observation of *Fermi*-LAT. We attempt to combine these results together to search for the ALP-photon oscillation effect and set constraint on the ALP parameter space.

This paper is structured as follows. In Sec. II, we briefly introduce the ALP-photon oscillation effect in the VHE astrophysical process and describe the propagation of the ALP-photon system in the blazar jet, extragalac-

tic space, and Milky Way. In Sec. III, we introduce the data fitting and statistical methods for this analysis. In Sec. IV, we investigate the ALP implication in the MAGIC observations of Mrk 421 and PG 1553+113. The conclusion is given in Sec. V.

II. THE OSCILLATION AND PROROGATION OF THE ALP-PHOTON SYSTEM

The Lagrangian of ALP including the effective ALP-photon interaction term is

$$\mathcal{L}_{\text{ALP}} = \frac{1}{2}\partial^\mu a \partial_\mu a - \frac{1}{2}m_a^2 a^2 - \frac{1}{4}g_{a\gamma} a F_{\mu\nu} \tilde{F}^{\mu\nu}, \quad (1)$$

where a is the ALP, m_a is its mass, $g_{a\gamma}$ is the coupling between the ALP and photons, and $F_{\mu\nu}$ and $\tilde{F}^{\mu\nu}$ are the electromagnetic field tensor and its dual tensor, respectively. The ALP-photon system propagating along the x_3 direction is written as [21] $\Psi = (A_1, A_2, a)^T$, where A_1 and A_2 denote the linear polarization amplitudes of the photon in the perpendicular directions. The corresponding density matrix $\rho = \Psi \otimes \Psi^\dagger$ satisfies the Von Neumann like equation [18]

$$i \frac{d\rho(x_3)}{dx_3} = [\rho(x_3), \mathcal{M}_0]. \quad (2)$$

Assuming that B_T is the transversal magnetic field aligned along the direction of x_2 , the mixing matrix \mathcal{M}_0 can be described by [13, 17, 22]

$$\mathcal{M}_0 = \begin{pmatrix} \Delta_{\text{pl}} + 2\Delta_{\text{QED}} & 0 & 0 \\ 0 & \Delta_{\text{pl}} + \frac{7}{2}\Delta_{\text{QED}} & \Delta_{a\gamma} \\ 0 & \Delta_{a\gamma} & \Delta_{aa} \end{pmatrix}, \quad (3)$$

with

$$\Delta_{\text{pl}} = -\frac{\omega_{\text{pl}}^2}{2E} \simeq -1.1 \times 10^{-4} \text{ kpc}^{-1} n_{\text{cm}^{-3}} E_{\text{GeV}}^{-1}, \quad (4)$$

$$\Delta_{\text{QED}} = \frac{\alpha E}{45\pi} \left(\frac{B_T}{B_{\text{cr}}} \right)^2 \simeq 4.1 \times 10^{-9} \text{ kpc}^{-1} E_{\text{GeV}} B_{\mu\text{G}}, \quad (5)$$

$$\Delta_{a\gamma} = \frac{1}{2} g_{a\gamma} B_T \simeq 1.52 \times 10^{-2} \text{ kpc}^{-1} g_{11} B_{\mu\text{G}}, \quad (6)$$

$$\Delta_{aa} = -\frac{m_a^2}{2E} \simeq -7.8 \times 10^{-2} \text{ kpc}^{-1} m_{\text{neV}}^2 E_{\text{GeV}}^{-1}, \quad (7)$$

where $\omega_{\text{pl}} = \sqrt{4\pi\alpha n_e/m_e}$ is the plasma frequency, n_e is the number density of the free electrons, α is the fine-structure constant, and $B_{\text{cr}} \equiv m_e^2/|e| \simeq 4.4 \times 10^{13} \text{ G}$. The terms Δ_{pl} and Δ_{QED} represent the plasma and QED vacuum polarisation effects, respectively. The notations $n_{\text{cm}^{-3}} \equiv n_e/1 \text{ cm}^{-3}$, $E_{\text{GeV}} \equiv E/1 \text{ GeV}$, $g_{11} \equiv g_{a\gamma}/10^{-11} \text{ GeV}^{-1}$, $B_{\mu\text{G}} \equiv B_T/1 \mu\text{G}$, and $m_{\text{neV}} \equiv m_a/1 \text{ neV}$ are used in above equations. The general mixing matrix \mathcal{M} depends on the angle ψ between the directions of B_T and x_2 .

The ALP-photon conversion would occur in numerous regions with different magnetic field configurations. The

final density matrix can be derived from the solution of Eq. (2) as

$$\rho(s) = T(s)\rho(0)T^\dagger(s). \quad (8)$$

The whole transfer matrix $T(s)$ for the propagation distance s reads

$$T(s) = \prod_i^n \mathcal{T}(i), \quad (9)$$

where $\mathcal{T}(i)$ can be derived from the mixing matrix $\mathcal{M}(i)$ in the i -th region. For the initial unpolarized photon beam with $\rho(0) = \text{diag}(1, 1, 0)/2$, the photon survival probability after propagation is given by [21]

$$P_{\gamma\gamma} = \text{Tr}((\rho_{11} + \rho_{22})T(s)\rho(0)T^\dagger(s)) \quad (10)$$

with $\rho_{ii} = \text{diag}(\delta_{i1}, \delta_{i2}, 0)$.

Then we describe the prorogation effect of the ALP-photon beam in three astrophysical regions with different magnetic field configurations, including the blazar jet, the extragalactic space, and the Milky Way [15, 28]. For the BL Lac objects considered in this work, we do not take into account the effects in the blazar broad line region. The ALP-photon oscillation might significantly occur in the BJMF. There are evidences that the magnetic field of the BL Lac jet can be described by the poloidal (along the jet, reads $B \propto r^{-2}$) and toroidal (perpendicular to the jet, reads $B \propto r^{-1}$) coherent components [55]. We take the BJMF model of the BL Lac sources as Refs. [26, 35].

The transverse magnetic field $B_{\text{jet}}(r)$ reads [56, 57]

$$B_{\text{jet}}(r) = B_0 \left(\frac{r}{r_{\text{VHE}}} \right)^{-1}, \quad (11)$$

where r_{VHE} is the distance between the central black hole and emission region. The density profile of the electrons $n_{\text{el}}(r)$ can be given by [58]

$$n_{\text{el}}(r) = n_0 \left(\frac{r}{r_{\text{VHE}}} \right)^{-2}. \quad (12)$$

Note that the above profiles hold in the jet comoving frame. The energies of the photons in the laboratory frame E_L and comoving frame E_j are related by the Doppler factor δ_D through $E_L = E_j \cdot \delta_D$.

The fit to the blazar spectra at multi-wave bands with the synchrotron self-Compton model could determine the values of the BJMF parameters. In our analysis, these parameters for one source during all the phases are assumed to be same. We set B_0 to be 0.1 G and 1.0 G for Mrk 421 and PG 1553+113, respectively, and take $\delta_D = 30$ and $n_0 = 3 \times 10^3 \text{ cm}^{-3}$ as the benchmark parameters. These values are consistent with the results derived in Refs. [53, 59]. In the region with $r > 1 \text{ kpc}$, we assume that the magnitude of BJMF is zero. Note that among the BJMF parameters r_{VHE} is difficult to determine through the measurements. Its value might range from

$\mathcal{O}(10^{16})$ - $\mathcal{O}(10^{17})$ cm. Here we adopt $r_{\text{VHE}} = 10^{17}$ cm as a benchmark parameter.

When the ALP-photon system propagates in the host galaxy in which the blazar is located, the oscillation effect can be neglected [35, 60]. If the blazar is located in a cluster with a rich environment, the turbulent inter-cluster magnetic field $\sim \mathcal{O}(1) \mu\text{G}$ may also induce a significant ALP-photon oscillation effect [28]. Since no definite evidences that the blazars Mrk 421 and PG 1553+113 are located in such environment have been provided, this oscillation effect is not considered in our analysis.

The oscillation in the extragalactic magnetic field on the largest cosmological scale is also neglected here. The magnitude of this magnetic field is not larger than $\mathcal{O}(1) \text{nG}$, while it is not precisely determined already [61]. For the VHE photons crossing in the extragalactic space, the attenuation effect caused by the extragalactic background light (EBL) through $\gamma_{\text{VHE}} + \gamma_{\text{EBL}} \rightarrow e^+ + e^-$ should be considered. This effect is described by a suppression factor of $e^{-\tau}$, where τ is the optical depth depending on the redshift of the source and the EBL density distribution. In this work, we take the EBL model provided by Ref. [62] as a benchmark. The redshift of Mrk 421 and PG 1553+113 are taken as $z_0 = 0.031$ and 0.45 , respectively.

Finally, we take into account the effect in the magnetic field of the Milky Way, where the ALPs could be reconverted to photons. Only the regular component of the Galactic magnetic field is considered here, while the random component on the small scale is neglected. The details of this model can be found in Ref. [63].

We show the photon survival probability $P_{\gamma\gamma}$ as a function of energy for the blazars Mrk 421 and PG 1553+113 in Fig. 1. It can be seen that the pure EBL attenuation effect described by the factor of $e^{-\tau}$ dramatically suppresses the photon energy spectrum at energies above $\mathcal{O}(10^2) \text{GeV}$. The ALP-photon oscillation might affect the survival probability at lower energies compared with the EBL attenuation effect. On the other hand, for some ALP parameters, the ALP-photon conversion could compensate the EBL attenuation effect at VHE region and lead to a moderate photon survival probability. This compensation may be significant for PG 1553+113 at large redshift as shown in Fig. 1.

III. GAMMA-RAY DATA FITTING AND STATISTICAL METHODS

MAGIC [64, 65] is a system containing two imaging atmospheric Cherenkov telescopes located at the Roque de los Muchachos Observatory in Spain. These telescopes could detect extensive air showers in stereoscopic mode, and observe VHE γ -ray sources at energies above 50GeV [54]. In Ref. [54], the MAGIC collaboration reported 32 VHE γ -ray spectra from 12 blazars. All the data were collected during dark nights in good weather conditions. The γ -ray spectra at lower energies $\sim 0.1 - 100 \text{GeV}$ dur-

ing the common operation time observed by *Fermi*-LAT are also analyzed in Ref. [54]. Here we use the MAGIC results of the BL Lac sources Mrk 421 and PG 1553+113 covering several activity phases to investigate the ALP-photon oscillation effects.

We take the expressions of the γ -ray blazar intrinsic energy spectra $\Phi_{\text{int}}(E)$ as Ref. [54]. $\Phi_{\text{int}}(E)$ can be described by some simple functions with three to five parameters, including the power law with exponential cut-off (EPWL), power law with superexponential cut-off (SEPWL), log parabola (LP), and log parabola with exponential cut-off (ELP). The functional expressions of $\Phi_{\text{int}}(E)$ are given as follows:

- EPWL:

$$\Phi_{\text{int}}(E) = F_0 \left(\frac{E}{E_0} \right)^{-\Gamma} \exp \left(-\frac{E}{E_c} \right), \quad (13)$$

- SEPWL:

$$\Phi_{\text{int}}(E) = F_0 \left(\frac{E}{E_0} \right)^{-\Gamma} \exp \left(-\left(\frac{E}{E_c} \right)^d \right), \quad (14)$$

- LP:

$$\Phi_{\text{int}}(E) = F_0 \left(\frac{E}{E_0} \right)^{-\Gamma - b \log \left(\frac{E}{E_0} \right)}, \quad (15)$$

- ELP:

$$\Phi_{\text{int}}(E) = F_0 \left(\frac{E}{E_0} \right)^{-\Gamma - b \log \left(\frac{E}{E_0} \right)} \exp \left(-\frac{E}{E_c} \right), \quad (16)$$

where F_0 , E_c , Γ , b , and d are free parameters. For EPWL and SEPWL, E_0 is taken to be 1GeV , while for LP and ELP, E_0 is also treated as a free parameter. For each phase, we choose the intrinsic energy spectrum with the minimum best-fit reduced χ^2 under the null hypothesis. This is different from the analysis in Ref. [45] where the expression of the intrinsic energy spectrum is same for all the phases. The spectrum expressions for all the phases adopted in this analysis are listed in Table I.

Under the alternative hypothesis including the ALP-photon oscillation effect, we obtain the expected photon spectrum as

$$\Phi_{\text{w ALP}}(E) = P_{\gamma\gamma} \Phi_{\text{int}}(E), \quad (17)$$

where $P_{\gamma\gamma}$ is the photon survival probability. The detected photon flux in the energy bin of (E_1, E_2) is given by [43, 45]

$$\Phi' = \frac{\int_0^\infty D(E', E_1, E_2) \Phi(E') dE'}{E_2 - E_1}, \quad (18)$$

where $D(E', E_1, E_2)$ is the energy dispersion function, and E' and $\Phi(E')$ are the energy and spectrum of the

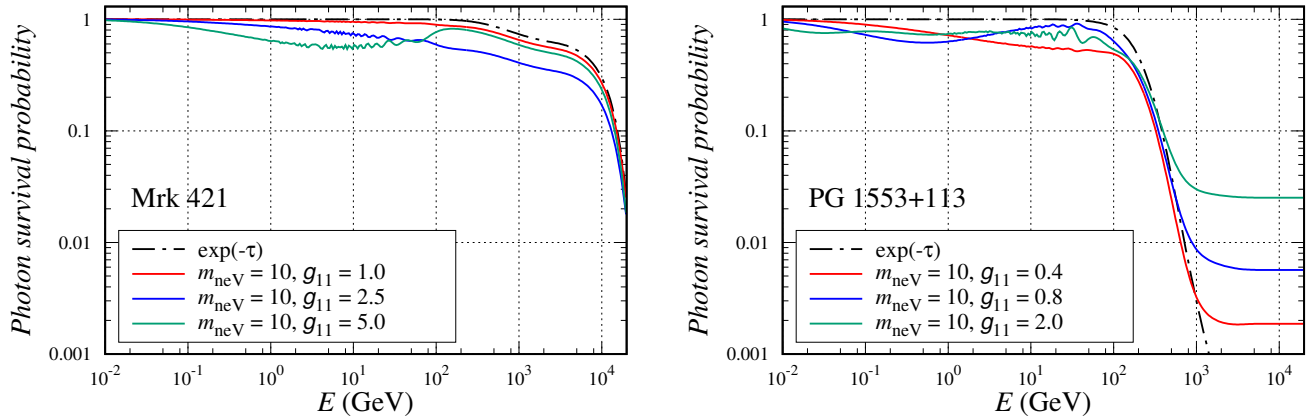


FIG. 1. Photon survival probability as a function of energy for Mrk 421 (left) and PG 1553+113 (right). The black dotted lines represent the survival probability with only the EBL attenuation effect. The solid lines represent the survival probability with both the EBL attenuation and ALP-photon oscillation effects for some selected ALP parameters. The EBL model is taken from Ref. [62].

TABLE I. The best-fit values of $\chi_{w/oALP}^2$ under the null hypothesis and χ_{min}^2 under the ALP hypothesis for all the phases. Periods stand for the corresponding MAGIC observations. The expressions of the intrinsic energy spectra, the effective d.o.f. of the TS distributions, and $\Delta\chi^2$ at 95% C.L. are also listed. The last two rows denote the results of the combined analysis.

Source [period]	Tstart	Tstop	Spectrum	$\chi_{w/oALP}^2$	χ_{min}^2	Effective d.o.f.	$\Delta\chi^2$
Mrk 421 [20130410]	2013-04-09T12:00	2013-04-10T12:00	SEPWL	12.244	8.845	4.45	10.232
Mrk 421 [20130411]	2013-04-10T18:00	2013-04-11T06:00	ELP	16.213	10.124	6.85	13.868
Mrk 421 [20130412]	2013-04-11T18:00	2013-04-12T06:00	ELP	8.911	6.186	7.54	14.868
Mrk 421 [20130413a]	2013-04-12T12:00	2013-04-13T12:00	ELP	16.007	12.928	8.00	15.527
Mrk 421 [20130413b]	2013-04-12T12:00	2013-04-13T12:00	SEPWL	9.733	8.645	4.72	10.657
Mrk 421 [20130413c]	2013-04-12T12:00	2013-04-13T12:00	SEPWL	10.049	7.537	4.56	10.406
Mrk 421 [20130414]	2013-04-13T12:00	2013-04-14T12:00	ELP	22.391	13.749	9.22	17.245
Mrk 421 [20130415a]	2013-04-14T21:17	2013-04-15T04:13	ELP	5.774	4.777	5.23	11.447
Mrk 421 [20130415b]	2013-04-14T21:17	2013-04-15T04:13	SEPWL	13.426	10.016	5.02	11.124
Mrk 421 [20130415c]	2013-04-14T21:17	2013-04-15T04:13	SEPWL	5.056	4.012	4.71	10.641
Mrk 421 [20130416]	2013-04-15T12:00	2013-04-16T09:00	SEPWL	32.863	19.552	5.48	11.829
Mrk 421 [20130417]	2013-04-16T18:00	2013-04-17T06:00	SEPWL	26.050	11.174	4.99	11.077
Mrk 421 [20130418]	2013-04-17T12:00	2013-04-18T12:00	EPWL	13.345	9.038	5.56	11.950
Mrk 421 [20130419]	2013-04-18T12:00	2013-04-19T12:00	ELP	3.609	1.964	4.07	9.625
Mrk 421 [20140426]	2014-04-25T18:00	2014-04-26T06:00	ELP	25.809	15.184	6.19	12.896
PG 1553+113 [ST0202]	2012-02-28T12:00	2012-03-04T12:00	EPWL	2.326	0.914	3.52	8.723
PG 1553+113 [ST0203]	2012-03-13T12:00	2012-05-02T12:00	SEPWL	15.598	6.342	6.24	12.970
PG 1553+113 [ST0302]	2013-04-07T12:00	2013-06-12T12:00	SEPWL	5.413	1.279	4.50	10.311
PG 1553+113 [ST0303]	2014-03-11T12:00	2014-03-25T12:00	EPWL	10.171	5.944	6.73	13.693
PG 1553+113 [ST0306]	2015-01-25T12:00	2015-08-07T12:00	SEPWL	4.704	0.718	3.43	8.578
Combined Mrk 421				221.480	204.554	31.17	45.206
Combined PG 1553+113				38.212	20.511	8.94	16.854

photons before detection, respectively. The energy resolution of MAGIC is taken to be 16% [65].

In Ref. [54], the *Fermi*-LAT spectra are provided in the form of spectral bow-ties rather spectral points. The bow-ties contain the information of the flux and local

spectrum index determined at the decorrelation energy; each one contributes two degrees of freedom in the fit.

The χ^2 of the fit is defined as [54]

$$\chi^2 = \left(\frac{\Phi'(E_{\text{LAT}}) - F_{\text{LAT}}}{\Delta F_{\text{LAT}}} \right)^2 + \left(\frac{\Gamma_{\text{fit}} - \Gamma_{\text{LAT}}}{\Delta \Gamma_{\text{LAT}}} \right)^2 + \sum_{i=1}^N \left(\frac{\Phi'(E_i) - \tilde{\phi}_i}{\delta_i} \right)^2, \quad (19)$$

where E_{LAT} , F_{LAT} , Γ_{LAT} , and Γ_{fit} are the central energy, flux, local spectral index, and the expected spectral index for the *Fermi*-LAT results, respectively. N is the number of the MAGIC spectral points, $\Phi'(E_i)$ is the expected flux of the photons, $\tilde{\phi}_i$ is the detected photon flux, and δ_i is the uncertainty of the MAGIC measurement.

With the χ^2 values under the ALP hypothesis in the $m_a - g_{a\gamma}$ plane, the constraint on the parameter space is set by requiring $\chi^2 \leq \chi_{\text{min}}^2 + \Delta\chi^2$, where χ_{min}^2 is the minimum best-fit χ^2 under the ALP hypothesis. Since the modifications of the balzar spectra nonlinearly depend on the ALP parameters, the threshold value of $\Delta\chi^2$ at the particular confidence level should be derived from the Monte Carlo simulations rather than directly using Wilks' theorem [28, 30]. Based on the best-fit spectra to the data under the null hypothesis, for each phase, 400 sets of spectra in the pseudo-experiments are generated by Gaussian samplings. The test statistic (TS) value is defined by the difference between the best-fit $\hat{\chi}^2$ under the null and ALP hypotheses for each generated spectrum $\text{TS} \equiv \hat{\chi}_{\text{null}}^2 - \hat{\chi}_{\text{w ALP}}^2$. In each phase, the distribution of TS for all the generated spectrum sets is derived. Such distribution can be described by the non-central χ^2 distribution with the non-centrality λ and the effective degree of freedom (d.o.f.). Although this TS distribution is derived under the null hypothesis, following Ref. [30] we take it as the approximation of the TS distribution under the ALP hypothesis and adopt the corresponding $\Delta\chi^2$ in the following analysis.

IV. CONSTRAINTS ON THE ALP PARAMETER SPACE

In this section, we investigate the implication of ALP for the observations of MAGIC and *Fermi*-LAT. The best-fit $\chi_{\text{w/oALP}}^2$ under the null hypothesis and $\chi_{\text{w ALP}}^2$ under the ALP hypothesis are given by Table I. We calculate the TS distributions for all the phases and obtain their non-centralities ~ 0.01 . The corresponding effective d.o.f. and the values of $\Delta\chi^2$ at 95% C.L. are also given by Table I.

The best-fit photon spectra under the null and ALP hypotheses for all the phases are shown in Fig. 2. We find that the null hypothesis can well fit the Mrk 421 observations. The corresponding best-fit reduced χ^2 are around an average value of 1.10. For the most of phases, introducing the ALP-photon oscillation would not significantly improve the fit. With the values of $\Delta\chi^2$, the constraints on the ALP parameter space at 95% C.L.

from the Mrk 421 observations are represented by the red contours in Fig. 3. We find that not all the observations of the single phase can be used to set the 95% C.L. constraint on the ALP parameter space. Following Ref. [45], we also perform an analysis combined the Mrk 421 results of the 15 phases. This approach could give a more reliable implication. The combined $\chi_{\text{w ALP}}^2$ in the $m_a - g_{a\gamma}$ plane and the best-fit value are shown in Fig. 3 and Table I, respectively. The red contour representing the combined upper limit at 95% C.L. is also shown.

In Fig. 4, the constraints on the ALP parameter space placed by CAST [66], the PKS 2155–304 observation of H.E.S.S. [23], and the NGC 1275 observation of *Fermi*-LAT [30] are shown for comparison. We also show the limits set by the analyses using the Mrk 421 observations of ARGO-YBJ and *Fermi*-LAT [45], and the PG 1553+113 observations of H.E.S.S. II and *Fermi*-LAT [43] in Fig. 4. Compared with the CAST constraint of $g_{a\gamma} \lesssim 6.6 \times 10^{-11} \text{ GeV}^{-1}$ [66], the combined limit at 95% C.L. set by this work excludes the ALP parameter region with the ALP-photon coupling of $g_{a\gamma} \gtrsim 2 \times 10^{-11} \text{ GeV}^{-1}$ for the ALP mass of $\sim 8 \times 10^{-9} \text{ eV} \lesssim m_a \lesssim 2 \times 10^{-7} \text{ eV}$. This combined constraint is not completely coincide with that derived from the observations of ARGO-YBJ and *Fermi*-LAT in Ref. [45]. A possible reason is that the spectral forms of the *Fermi*-LAT results are different in these two analyses. The spectral points of the *Fermi*-LAT result provide a large contributions to the final χ^2 in Ref. [45]. On the other hand, the *Fermi*-LAT results used in this analysis are in the form of bow-ties with two parameters. Therefore, the VHE data from MAGIC would provide the dominant contributions to the final χ^2 in this analysis. Additionally, the intrinsic energy spectra for all the phases are assumed to be same in Ref. [45], while they are separately chosen according the fits for different phases in this analysis. This difference would also induce different fitting results.

For PG 1553+113, the best-fit reduced χ^2 are around an average value of 1.23. For the phases except PG 1553+113 [ST0203], the ALP hypothesis does not significantly improve the fit. However, for PG 1553+113 [ST0203], the difference between the best-fit χ^2 values under the null and ALP hypotheses is near the threshold $\Delta\chi^2$ at 95% C.L. as shown in Table I. Combining all results of the 5 phases, we find that this difference becomes larger than $\Delta\chi^2$ at 95% C.L. In this case, we only show the values of χ^2 in the $m_a - g_{a\gamma}$ plane in Fig. 5, but do not set the constraints on the ALP parameter space.

Some comments on these results are given as follows. The ALP-photon oscillation effect strongly depends on the magnitude of the astrophysical magnetic field. For PG 1553+113, we take a relative large value of $B_0 = 1 \text{ G}$, which directly enhances the oscillation effect. Since the ALPs do not interact with the EBL, the large oscillation effect could compensate the attenuation effect and reduce the absorption of the VHE photons in the extragalactic space, especially for the astrophysical source at large redshift suffering from a significant attenuation

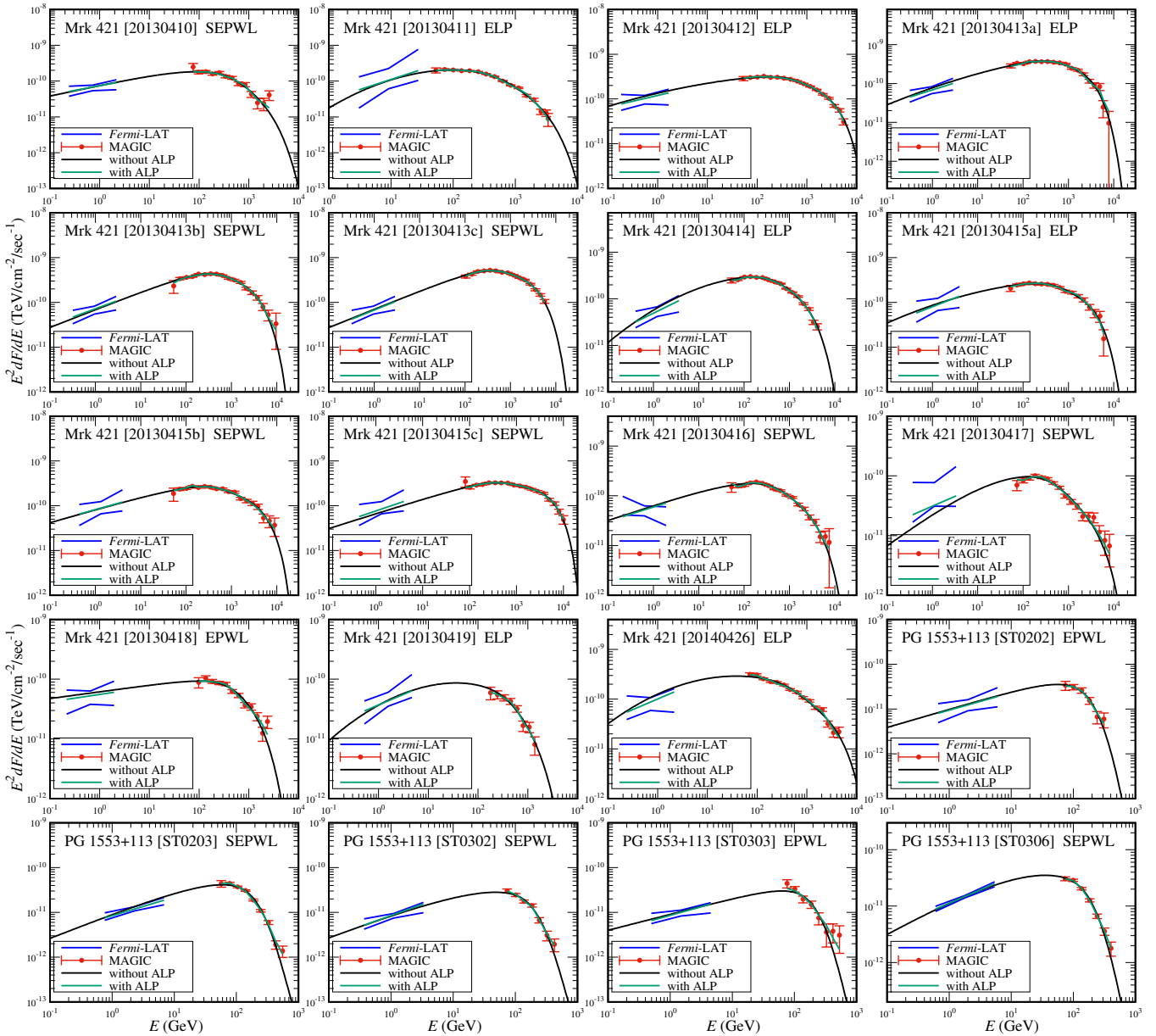


FIG. 2. Best-fit photon spectra for the 15 and 5 phases of Mrk 421 and PG 1553+113, respectively. The black and green lines represent the spectra under the null and ALP hypotheses, respectively. The values of the corresponding best-fit χ^2 are listed in Table I. The spectral points and bow-ties represent the results from MAGIC and *Fermi*-LAT [54], respectively.

effect. Therefore, for PG 1553+113 at $z_0 \sim 0.45$, the oscillation effect might induce a relative large photon flux at VHE band compared with the null hypothesis. From Fig. 2, we can see that the ALP hypothesis improves the fit to the last one or two data points of the MAGIC measurements, which seem not to drop dramatically compared with the perivenous data points. This behavior can be explicitly seen in the spectrum of the phase PG 1553+113 [ST0303], despite the uncertainties of this phase are relative large. On the other hand, the spectrum of the phase PG 1553+113 [ST0203] has small uncertainties and could be used to reveal the oscillation

effect.

We emphasize that the results discussed above are affected by the astrophysical uncertainties. The dominant uncertainties are from the BJMF model. In the BJMF model used in this work, the magnitude of the magnetic field depends on the parameters B_0 , δ_D , n_0 , and r_{VHE} . As discussed in Refs. [28, 45], the distance between the VHE emission site and the central black hole r_{VHE} , and the magnitude of the core magnetic field B_0 at r_{VHE} would significantly affect final results. The parameter B_0 directly characterizes the magnitude of the BJMF. In principle, this parameter can be obtained from the fit to

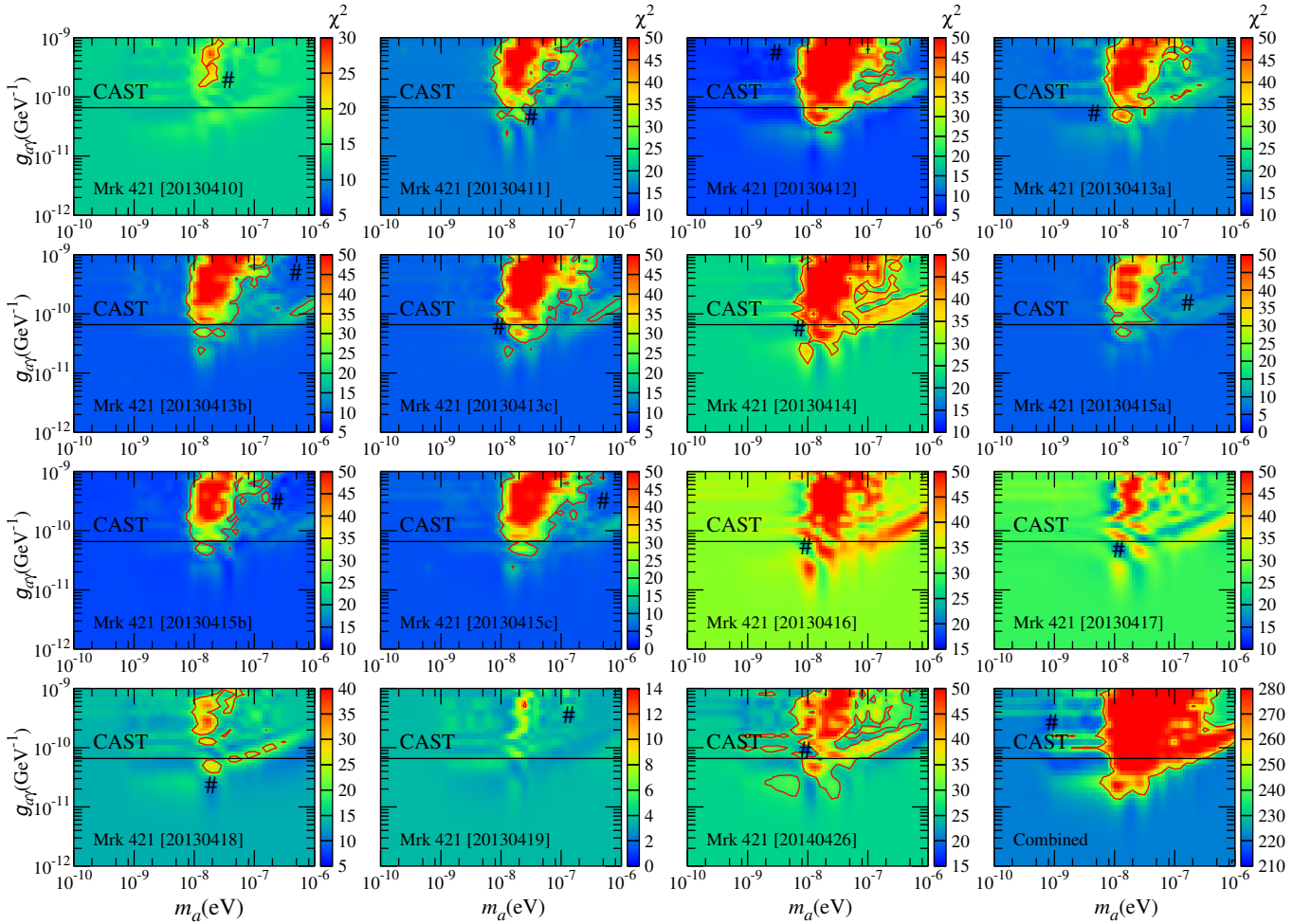


FIG. 3. $\chi_{w,ALP}^2$ values in the $m_a - g_{a\gamma}$ plane for the 15 phases of Mrk 421. The $\chi_{w,ALP}^2$ values for the combined results are shown in the bottom right panel. The red contours represent the excluded regions at 95% C.L. The “#” symbols represent the best-fit ALP parameter points. The horizontal line represents the upper limit placed by CAST [66].

the blazar spectrum using the synchrotron self-Compton model. However, the value of r_{VHE} is difficult to precisely determine.

As discussed in Ref. [45], for the increasing value of r_{VHE} in the range of $\sim 10^{16} - 10^{18}$ cm, the final constraint from the Mrk 421 observations would also become more strict by a magnitude of 1–2 orders. The results for Mrk 421 in this analysis have similar dependence on r_{VHE} . For PG 1553+113, we perform an analysis for a small value of r_{VHE} as 3×10^{16} cm. We find that the difference between the best-fit χ^2 under the null and ALP hypotheses is 17.068, which is slightly larger than the threshold value at 95% C.L. of 16.587. In this case, since the ALP hypothesis is able to improve the fit, the constraint on the parameter space is not set. The corresponding χ^2 under the ALP hypothesis for PG 1553+113 are shown in Fig. 6. We can see that for the fixed m_a , the behavior of the change of χ^2 for $r_{VHE} = 3 \times 10^{16}$ cm is similar with that at smaller $g_{a\gamma}$ for $r_{VHE} = 10^{17}$ cm.

V. CONCLUSION

In this work, we analyze the ALP-photon oscillation effect in the spectra of the blazars Mrk 421 and PG 1553+113 measured by MAGIC and *Fermi*-LAT during the common operation time, that covers the 15 and 5 activity phases, respectively. We find that not all the observations of these phases can be individually used to set the 95% C.L. limit on the ALP parameter space. For Mrk 421, we find that the constraint can be significantly improved if the results of all the 15 phases are combined. The combined Mrk 421 observations of MAGIC and *Fermi*-LAT have excluded the ALP parameter region with the ALP-photon coupling of $g_{a\gamma} \gtrsim 2 \times 10^{-11} \text{ GeV}^{-1}$ for the ALP mass of $\sim 8 \times 10^{-9} \text{ eV} \lesssim m_a \lesssim 2 \times 10^{-7} \text{ eV}$ at 95% C.L. For PG 1553+113, we find that the ALP hypothesis can slightly improve the fit to the data in some parameter regions. However, since the anomalies of the intrinsic spectrum and the EBL model may also induce the similar effect, we do not make a further ALP inter-

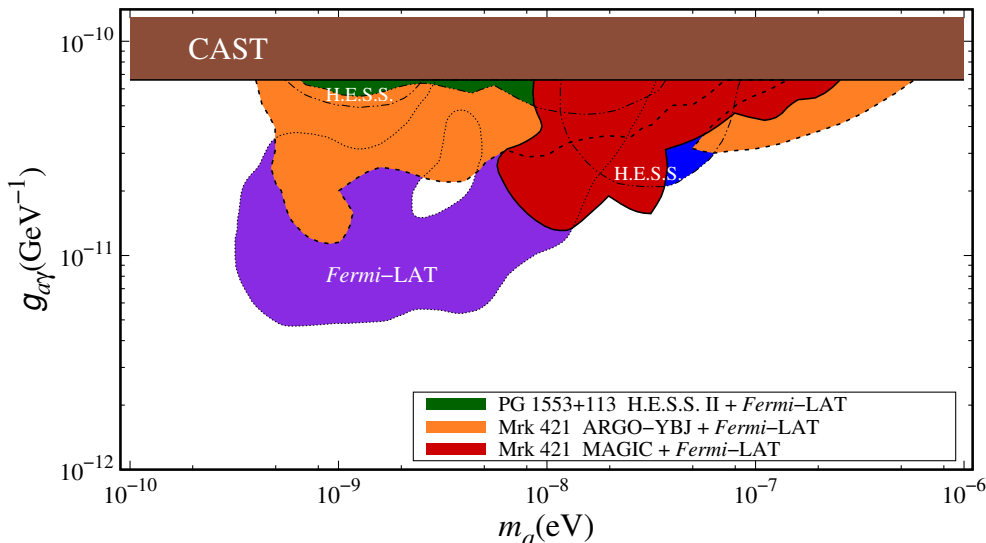


FIG. 4. 95% C.L. upper limit (red contour) placed by the Mrk 421 observations of MAGIC and *Fermi*-LAT. The upper limits set by CAST [66], the PKS 2155–304 observation of H.E.S.S. [23], and the NGC 1275 observation of *Fermi*-LAT [30] are shown for comparison. The limits placed by the analyses using the Mrk 421 observations of ARGO-YBJ and *Fermi*-LAT [45], and the PG 1553+113 observations of H.E.S.S. II and *Fermi*-LAT [43] are also shown.

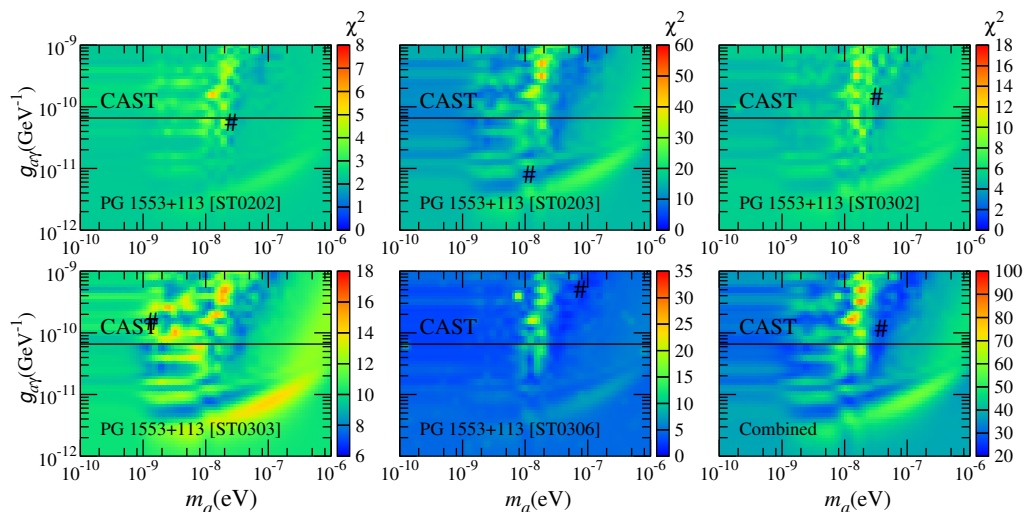


FIG. 5. $\chi^2_{w,ALP}$ values in the $m_a - g_{a\gamma}$ plane for the 5 phases of PG 1553+113. The $\chi^2_{w,ALP}$ values for the combined results are shown in the bottom right panel. The “#” symbols represent the best-fit ALP parameter points. The horizontal line represents the upper limit placed by CAST [66].

pretation for the current observation.

In the future, the new generation VHE γ -ray observations, such as Cherenkov Telescope Array [67], Large High Altitude Air Shower Observatory [68], High Energy cosmic-Radiation Detection [69], Gamma-Astronomy Multifunction Modules Apparatus [70], and Tunka Advanced Instrument for Gamma-ray and Cosmic ray Astrophysics-Hundred Square km Cosmic Origin Explorer [71], will collect more data for the high energy γ -ray sources at large distances from the Earth with high precision. With these precise γ -ray observations for

several blazars, it is possible to test the ALP-photon oscillation at the VHE band or set the more stringent constraints on the ALP parameters.

ACKNOWLEDGMENTS

The authors would like to thank Mireia Nieves Rosillo for providing the energy spectra of Mrk 421 and PG 1553+113 measured by MAGIC and *Fermi*-LAT in the common operation time. We also thank Jun-Guang

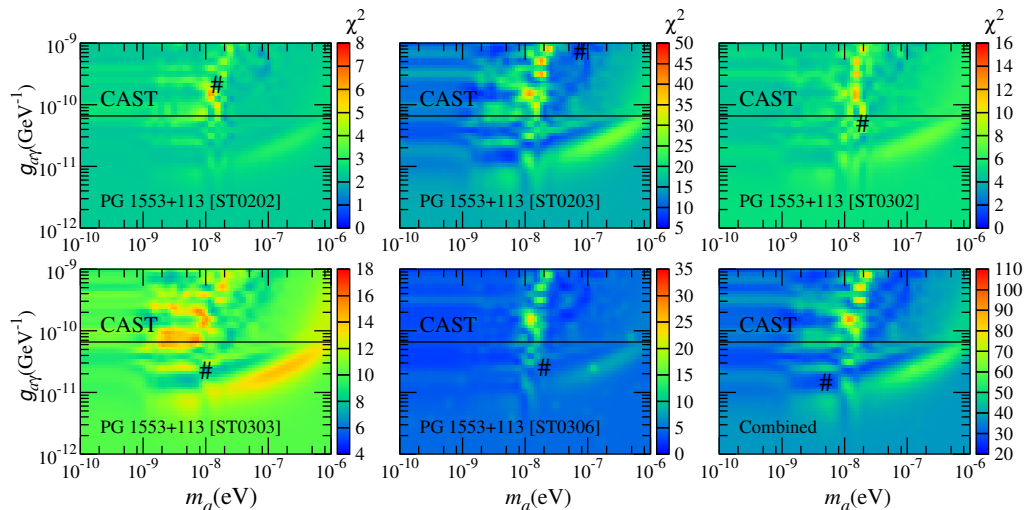


FIG. 6. Same as Fig. 5 but for $r_{\text{VHE}} = 3 \times 10^{16}$ cm.

Guo for providing helpful discussions and comments. This work is supported by the National Key R&D Pro-

gram of China (Grant No. 2016YFA0400200) and the National Natural Science Foundation of China (Grants No. U1738209 and No. 11851303).

-
- [1] R. Peccei and H. R. Quinn, *Phys. Rev. D* **16**, 1791 (1977).
[2] R. Peccei and H. R. Quinn, *Phys. Rev. Lett.* **38**, 1440 (1977).
[3] S. Weinberg, *Phys. Rev. Lett.* **40**, 223 (1978).
[4] F. Wilczek, *Phys. Rev. Lett.* **40**, 279 (1978).
[5] J. Preskill, M. B. Wise, and F. Wilczek, *Phys. Lett. B* **120**, 127 (1983).
[6] L. Abbott and P. Sikivie, *Phys. Lett. B* **120**, 133 (1983).
[7] M. Dine and W. Fischler, *Phys. Lett. B* **120**, 137 (1983).
[8] M. Khlopov, A. Sakharov, and D. Sokoloff, *Nucl. Phys. B Proc. Suppl.* **72**, 105 (1999).
[9] P. Sikivie, *Int. J. Mod. Phys. A* **25**, 554 (2010), arXiv:0909.0949 [hep-ph].
[10] P. Svrcek and E. Witten, *JHEP* **06**, 051 (2006), arXiv:hep-th/0605206.
[11] A. Arvanitaki, S. Dimopoulos, S. Dubovsky, N. Kaloper, and J. March-Russell, *Phys. Rev. D* **81**, 123530 (2010), arXiv:0905.4720 [hep-th].
[12] D. J. E. Marsh, *Phys. Rept.* **643**, 1 (2016), arXiv:1510.07633 [astro-ph.CO].
[13] G. Raffelt and L. Stodolsky, *Phys. Rev. D* **37**, 1237 (1988).
[14] A. De Angelis, M. Roncadelli, and O. Mansutti, *Phys. Rev. D* **76**, 121301 (2007), arXiv:0707.4312 [astro-ph].
[15] D. Hooper and P. D. Serpico, *Phys. Rev. Lett.* **99**, 231102 (2007), arXiv:0706.3203 [hep-ph].
[16] M. Simet, D. Hooper, and P. D. Serpico, *Phys. Rev. D* **77**, 063001 (2008), arXiv:0712.2825 [astro-ph].
[17] A. Mirizzi, G. G. Raffelt, and P. D. Serpico, *Phys. Rev. D* **76**, 023001 (2007), arXiv:0704.3044 [astro-ph].
[18] A. Mirizzi and D. Montanino, *JCAP* **12**, 004 (2009), arXiv:0911.0015 [astro-ph.HE].
[19] A. V. Belikov, L. Goodenough, and D. Hooper, *Phys. Rev. D* **83**, 063005 (2011), arXiv:1007.4862 [astro-ph.HE].
[20] A. Dominguez, M. A. Sanchez-Conde, and F. Prada, *JCAP* **11**, 020 (2011), arXiv:1106.1860 [astro-ph.CO].
[21] A. De Angelis, G. Galanti, and M. Roncadelli, *Phys. Rev. D* **84**, 105030 (2011), [Erratum: *Phys. Rev. D* **87**, 109903 (2013)], arXiv:1106.1132 [astro-ph.HE].
[22] D. Horns, L. Maccione, M. Meyer, A. Mirizzi, D. Montanino, and M. Roncadelli, *Phys. Rev. D* **86**, 075024 (2012), arXiv:1207.0776 [astro-ph.HE].
[23] A. Abramowski et al. (H.E.S.S.), *Phys. Rev. D* **88**, 102003 (2013), arXiv:1311.3148 [astro-ph.HE].
[24] M. Meyer, D. Horns, and M. Raue, *Phys. Rev. D* **87**, 035027 (2013), arXiv:1302.1208 [astro-ph.HE].
[25] O. Mena and S. Razzaque, *JCAP* **11**, 023 (2013), arXiv:1306.5865 [astro-ph.HE].
[26] F. Tavecchio, M. Roncadelli, and G. Galanti, *Phys. Lett. B* **744**, 375 (2015), arXiv:1406.2303 [astro-ph.HE].
[27] M. Meyer and J. Conrad, *JCAP* **12**, 016 (2014), arXiv:1410.1556 [astro-ph.HE].
[28] M. Meyer, D. Montanino, and J. Conrad, *JCAP* **09**, 003 (2014), arXiv:1406.5972 [astro-ph.HE].
[29] R. Reesman and T. Walker, *JCAP* **08**, 021 (2014), arXiv:1402.2533 [astro-ph.HE].
[30] M. Ajello et al. (Fermi-LAT), *Phys. Rev. Lett.* **116**, 161101 (2016), arXiv:1603.06978 [astro-ph.HE].
[31] B. Berenji, J. Gaskins, and M. Meyer, *Phys. Rev. D* **93**, 045019 (2016), arXiv:1602.00091 [astro-ph.HE].
[32] M. Meyer, M. Giannotti, A. Mirizzi, J. Conrad, and M. Sánchez-Conde, *Phys. Rev. Lett.* **118**, 011103 (2017), arXiv:1609.02350 [astro-ph.HE].
[33] K. Kohri and H. Kodama, *Phys. Rev. D* **96**, 051701 (2017), arXiv:1704.05189 [hep-ph].
[34] J. Majumdar, F. Calore, and D. Horns, *PoS IFS2017*, 168 (2017), arXiv:1711.08723 [hep-ph].

- [35] G. Galanti, F. Tavecchio, M. Roncadelli, and C. Evoli, *Mon. Not. Roy. Astron. Soc.* **487**, 123 (2019), [arXiv:1811.03548 \[astro-ph.HE\]](#).
- [36] G. Galanti and M. Roncadelli, *JHEAp* **20**, 1 (2018), [arXiv:1805.12055 \[astro-ph.HE\]](#).
- [37] G. Galanti and M. Roncadelli, *Phys. Rev. D* **98**, 043018 (2018), [arXiv:1804.09443 \[astro-ph.HE\]](#).
- [38] C. Zhang, Y.-F. Liang, S. Li, N.-H. Liao, L. Feng, Q. Yuan, Y.-Z. Fan, and Z.-Z. Ren, *Phys. Rev. D* **97**, 063009 (2018), [arXiv:1802.08420 \[hep-ph\]](#).
- [39] Y.-F. Liang, C. Zhang, Z.-Q. Xia, L. Feng, Q. Yuan, and Y.-Z. Fan, *JCAP* **06**, 042 (2019), [arXiv:1804.07186 \[hep-ph\]](#).
- [40] M. Libanov and S. Troitsky, *Phys. Lett. B* **802**, 135252 (2020), [arXiv:1908.03084 \[astro-ph.HE\]](#).
- [41] G. Long, W. Lin, P. Tam, and W. Zhu, *Phys. Rev. D* **101**, 063004 (2020), [arXiv:1912.05309 \[astro-ph.HE\]](#).
- [42] X.-J. Bi, Y. Gao, J. Guo, N. Houston, T. Li, F. Xu, and X. Zhang, *Phys. Rev. D* **103**, 043018 (2021), [arXiv:2002.01796 \[astro-ph.HE\]](#).
- [43] J. Guo, H.-J. Li, X.-J. Bi, S.-J. Lin, and P.-F. Yin, *Chin. Phys. C* **45**, 025105 (2021), [arXiv:2002.07571 \[astro-ph.HE\]](#).
- [44] R. Buehler, G. Gallardo, G. Maier, A. Domínguez, M. López, and M. Meyer, *JCAP* **09**, 027 (2020), [arXiv:2004.09396 \[astro-ph.HE\]](#).
- [45] H.-J. Li, J.-G. Guo, X.-J. Bi, S.-J. Lin, and P.-F. Yin, *Phys. Rev. D* **103**, 083003 (2021), [arXiv:2008.09464 \[astro-ph.HE\]](#).
- [46] J.-G. Cheng, Y.-J. He, Y.-F. Liang, R.-J. Lu, and E.-W. Liang, *Phys. Lett. B* **821**, 136611 (2021), [arXiv:2010.12396 \[astro-ph.HE\]](#).
- [47] Y.-F. Liang, X.-F. Zhang, J.-G. Cheng, H.-D. Zeng, Y.-Z. Fan, and E.-W. Liang, *JCAP* **11**, 030 (2021), [arXiv:2012.15513 \[astro-ph.HE\]](#).
- [48] G. Long, S. Chen, S. Xu, and H.-H. Zhang, *Phys. Rev. D* **104**, 083014 (2021), [arXiv:2101.10270 \[astro-ph.HE\]](#).
- [49] J. Davies, M. Meyer, and G. Cotter, *Phys. Rev. D* **103**, 023008 (2021), [arXiv:2011.08123 \[astro-ph.HE\]](#).
- [50] J. Zhou, Z. Wang, F. Huang, and L. Chen, *JCAP* **08**, 007 (2021), [arXiv:2102.05833 \[astro-ph.HE\]](#).
- [51] I. Batković, A. De Angelis, M. Doro, and M. Manganaro, *Universe* **7**, 185 (2021), [arXiv:2106.03424 \[astro-ph.HE\]](#).
- [52] H. Abdalla et al. (H.E.S.S., LAT), *Astron. Astrophys.* **600**, A89 (2017), [arXiv:1612.01843 \[astro-ph.HE\]](#).
- [53] B. Bartoli et al. (ARGO-YBJ), *Astrophys. J. Suppl.* **222**, 6 (2016), [arXiv:1511.06851 \[astro-ph.HE\]](#).
- [54] V. Acciari et al. (MAGIC), *Mon. Not. Roy. Astron. Soc.* **486**, 4233 (2019), [arXiv:1904.00134 \[astro-ph.HE\]](#).
- [55] R. Pudritz, M. Hardcastle, and D. Gabuzda, *Space Sci. Rev.* **169**, 27 (2012), [arXiv:1205.2073 \[astro-ph.HE\]](#).
- [56] M. C. Begelman, R. D. Blandford, and M. J. Rees, *Rev. Mod. Phys.* **56**, 255 (1984).
- [57] G. Ghisellini and F. Tavecchio, *Mon. Not. Roy. Astron. Soc.* **397**, 985 (2009), [arXiv:0902.0793 \[astro-ph.CO\]](#).
- [58] S. P. O'Sullivan and D. C. Gabuzda, *Mon. Not. Roy. Astron. Soc.* **400**, 26 (2009), [arXiv:0907.5211 \[astro-ph.CO\]](#).
- [59] A. Celotti and G. Ghisellini, *Mon. Not. Roy. Astron. Soc.* **385**, 283 (2008), [arXiv:0711.4112 \[astro-ph\]](#).
- [60] F. Tavecchio, M. Roncadelli, G. Galanti, and G. Bonnoli, *Phys. Rev. D* **86**, 085036 (2012), [arXiv:1202.6529 \[astro-ph.HE\]](#).
- [61] P. Ade et al. (Planck), *Astron. Astrophys.* **594**, A19 (2016), [arXiv:1502.01594 \[astro-ph.CO\]](#).
- [62] A. Franceschini, G. Rodighiero, and M. Vaccari, *Astron. Astrophys.* **487**, 837 (2008), [arXiv:0805.1841 \[astro-ph\]](#).
- [63] R. Jansson and G. R. Farrar, *Astrophys. J. Lett.* **761**, L11 (2012), [arXiv:1210.7820 \[astro-ph.GA\]](#).
- [64] J. Aleksić et al., *Astropart. Phys.* **72**, 61 (2016), [arXiv:1409.6073 \[astro-ph.IM\]](#).
- [65] J. Aleksić et al. (MAGIC), *Astropart. Phys.* **72**, 76 (2016), [arXiv:1409.5594 \[astro-ph.IM\]](#).
- [66] V. Anastassopoulos et al. (CAST), *Nature Phys.* **13**, 584 (2017), [arXiv:1705.02290 \[hep-ex\]](#).
- [67] B. Acharya et al. (CTA Consortium), *Astropart. Phys.* **43**, 3 (2013).
- [68] Z. Cao (LHAASO), *Chin. Phys. C* **34**, 249 (2010).
- [69] X. Huang et al., *Astropart. Phys.* **78**, 35 (2016), [arXiv:1509.02672 \[astro-ph.HE\]](#).
- [70] A. E. Egorov, N. P. Topchiev, A. M. Galper, O. D. Dalkarov, A. A. Leonov, S. I. Suchkov, and Y. T. Yurkin, *JCAP* **11**, 049 (2020), [arXiv:2005.09032 \[astro-ph.HE\]](#).
- [71] L. A. Kuzmichev et al., *Phys. Atom. Nucl.* **81**, 497 (2018).